


Steady-State Fluorescence of Highly Absorbing Samples in Transmission Geometry: A Simplified Quantitative Approach Considering Reabsorption Events

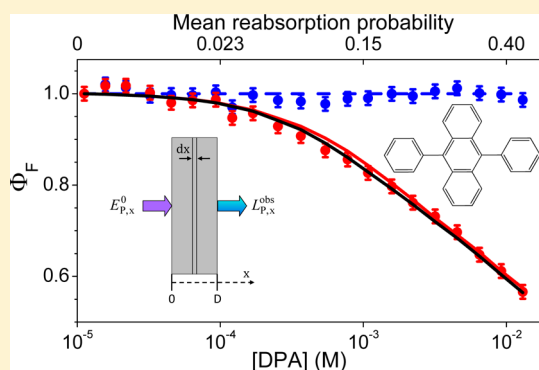
Nicolás I. Krimer,[†] Darío Rodrigues,[†] Hernán B. Rodríguez,^{‡,§} and Martín Mirenda^{*,†,§} 

[†]Gerencia Química, Centro Atómico Constituyentes, Comisión Nacional de Energía Atómica (CNEA-CONICET), Av. Gral. Paz 1499, B1650KNA San Martín, Buenos Aires, Argentina

[‡]Instituto de Investigaciones Fisicoquímicas Teóricas y Aplicadas (INIFTA, UNLP-CONICET), Facultad de Ciencias Exactas, Universidad Nacional de La Plata, Casilla de Correo 16, Sucursal 4, (1900) La Plata, Argentina

[§]Departamento de Química Inorgánica, Analítica y Química Física, Facultad de Ciencias Exactas y Naturales, Universidad de Buenos Aires, Ciudad Universitaria, Pab. II, C1428EHA, Buenos Aires, Argentina

ABSTRACT: A simplified methodology to acquire steady-state emission spectra and quantum yields of highly absorbing samples is presented. The experimental setup consists of a commercial spectrofluorometer adapted to transmission geometry, allowing the detection of the emitted light at 180° with respect to the excitation beam. The procedure includes two different mathematical approaches to describe and reproduce the distortions caused by reabsorption on emission spectra and quantum yields. Toluene solutions of 9,10-diphenylanthracene, DPA, with concentrations ranging between 1.12×10^{-5} and 1.30×10^{-2} M, were used to validate the proposed methodology. This dye has significant probability of reabsorption and re-emission in concentrated solutions without showing self-quenching or aggregation phenomena. The results indicate that the reabsorption corrections, applied on molecular emission spectra and quantum yields of the samples, accurately reproduce experimental data. A further discussion is performed concerning why the re-emitted radiation is not detected in the experiments, even at the highest DPA concentrations.



Experimental measurements of steady-state emission spectra and quantum yields in highly absorbing media do not represent simple tasks due to the occurrence of inner-filter effects.^{1,2} An excitation or primary inner-filter effect takes place when the excitation light is mainly absorbed at the surface of the optical cell, avoiding its penetration into the sample. On the other hand, emission or secondary inner-filter events—also commonly referred to as radiative energy transfer, trivial energy transfer, or simply reabsorption—take place when the emitted light is reabsorbed, as it passes through the sample toward the detector, as a consequence of the overlap between the emission and the absorption spectra. As such, both effects are sources of spectral distortions and lowering of the total emission intensity, leading to underestimations of emission quantum yields. Moreover, in some cases, reabsorbed light can be re-emitted and further detected, causing an increment in the observed emission intensity at longer wavelengths. In this case, an overestimation of the emission quantum yields can be obtained. The magnitude of these events strongly depends on: (a) the geometry of the excitation and the emission detection, (b) the optical path length and the geometry of the sample cell, (c) the concentration of the absorbing substance, and (d) the overlap between absorption and emission spectra.³

In the past, this problem was addressed for the three most common irradiation/detection geometries: (a) *front-face* or *reflection geometry*, in which the emission is collected at the same side in which the sample is irradiated; (b) *90°* or *right-angle geometry*, in which the emission is detected along a direction perpendicular to the incident beam after it passes through the sample; and (c) *transmission geometry*, in which the emission is collected from the opposite side at which it is excited.⁴

For example, *front-face geometry* was the configuration chosen by Vavilov⁵ in the early 1900s to assess the extinction of fluorescence in highly concentrated dye solutions. Later, Budó et al.^{6–8} and Melhuish⁹ performed absolute emission quantum yield measurements of a large number of substances using this geometry followed by sophisticated mathematical corrections to compensate reabsorption and re-emission effects. Rohatgi and Singhal,^{10,11} Eisinger and Flores,¹² Lopez Arbeloa,¹³ and Vieira Ferreira et al.,¹⁴ among others, have also devised alternative and valuable contributions over

Received: July 22, 2016

Accepted: December 5, 2016

Published: December 5, 2016

the years. However, the *front-face geometry* has the disadvantage that the penetration of the excitation light into the sample diminishes as the absorbance is increased, changing the spatial volume in which the fluorescence is generated. Moreover, these measures are often extremely sensitive to small changes in incidence and detection angles, which make them difficult to be performed.

Measurements using the 90° geometry began to be popular after the work of Weber and Teale.¹⁵ Over the years, a lot of effort was invested by several authors in order to obtain mathematical expressions capable to correct reabsorption and re-emission effects in this geometry.^{16–21} Gu and Kenny^{22,23} reviewed the subject a short time ago for commercial spectrofluorometers, including converging lenses and small pinholes in both the excitation and emission beams. Similarly to what happens with the *front-face geometry*, the difficulty in this case arises in the accurate determination of the amount of excitation light that is absorbed in the detection volume, principally in highly absorbing samples. An interesting advance on this issue constitutes the use of horizontal slits, as was recently reported by Fonin et al.²⁴ This feature ensures the complete overlap between absorption and detection volumes, even for high optical densities. Although the exciting radiation is totally absorbed after a few microns for highly absorbing samples, the authors do not report problems associated with internal reflections at the cell edges, which were previously mentioned by other authors.¹⁷ Under this configuration the primary inner-filter effects are avoided, although an integrated reabsorption correction is still necessary by considering that neither re-emission nor emission of another entity (dimer, excimer, etc.) appears at the red edge of the spectrum.

The *transmission geometry* constitutes the less explored configuration. Although mentioned in several classical texts,^{25,26} its rare implementation is probably related to the possibility of excitation light reaching and damaging the detector. However, this configuration has a geometric advantage compared with the other geometries because, for collimated parallel excitation and emission beams, it ensures the complete overlap between the excitation and detection volumes.

Current commercial spectrofluorometers exhibit extra geometric complexities compared with older ones, most notably those related to the presence of convergent lenses, which are included by the manufacturers in order to maximize the emission signal coming from very dilute analytes. These lenses focus the excitation light and enable the detection of the emission from a very small sample volume, allowing an increment in the fluorescence detection limit. However, this new beam trace introduces additional difficulties to account for inner-filter effects, especially for nontransmission geometries.

Along the years, quantitative fluorometry has been proved to be fundamental in many areas of science, including analytical chemistry,²⁷ biology,²⁸ and materials,²⁹ among others. As such, the accurate consideration of inner-filter effects is indispensable for measurements in highly absorbing samples because the emitted light intensity becomes not proportional to the absorbed light and, therefore, becomes not proportional to the analytical concentration. The lack of attention on these phenomena may even induce misinterpretations of the experimental data.^{30,31}

A simplified procedure to obtain steady-state emission spectra and fluorescence quantum yields, Φ_F , of highly absorbing dye solutions is presented in this work. The

experimental measurements were performed on a commercial spectrofluorometer adapted to transmission geometry. The dye chosen to validate the methodology was 9,10-diphenylanthracene, DPA, which has a Φ_F value close to unity in toluene.³² The considerable overlap between the absorption and emission spectra makes reabsorption and re-emission events significant for highly concentrated DPA solutions.³³ On the other hand, no self-quenching or aggregation phenomena were reported for this dye in a wide concentration range.⁴ The present methodology includes both spectral and Φ_F corrections by means of two different mathematical approaches describing reabsorption events. The evaluation of these models is achieved by comparing the experimental spectra and Φ_F values with calculated ones. A further discussion, concerning why the re-emitted radiation is not detected in the present measurement geometry, is also included.

EXPERIMENTAL SECTION

Chemicals. DPA (97%) was purchased from Aldrich and used as received. DPA solutions from 1.12×10^{-5} to 1.30×10^{-2} M were prepared by dissolving the reagent in degassed toluene (Fluka, puriss. p.a., ACS reagent, $\geq 99.7\%$ GC). The solutions were sonicated during 30 min to ensure complete dissolution, and were left in the dark for one night before use. Quinine bisulfate, QBS (analytical reagent, purity $>99\%$), was purchased from Fluka and used as received. A 7.6×10^{-5} M acidic aqueous solution of QBS was prepared by dissolving the reagent in H_2SO_4 0.5 M (Merck, 95–97%, for analysis). Deionized water ($18 \text{ M}\Omega \times \text{cm}$, obtained from a Milli-Q system) was used for preparing the solution, which was left in the dark for one night before use.

Figure 1 shows the normalized absorption and emission spectra of a diluted DPA solution, together with the

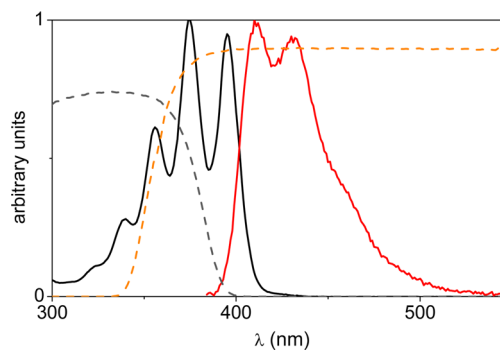


Figure 1. Normalized absorption (black line) and emission (red line) spectra of DPA in toluene and transmission spectra of Schott UG11 (dashed grey line) and WG360 (dashed orange line) optical filters.

transmission spectra of the optical filters used in the experiments (see below). DPA shows substantial spectral overlap, with absorption and emission maxima at 375 ($\epsilon = 1.31 \times 10^4 \text{ M}^{-1} \text{ cm}^{-1}$) and 410 nm, respectively.^{34,35}

Measurements. Absorption measurements were performed in a Cary 50 Conc UV–vis spectrophotometer (Varian), equipped with a thermostated sample-holder. The bandwidth of the excitation slit was 1.5 nm.

Steady-state fluorescence spectra were recorded in a PTI QuantaMaster 4 CW fluorometer, equipped with a xenon short-arc lamp UXL-75XE and a thermostated sample-holder. Both excitation and emission monochromators show gratings of

1200 line/mm, in which 1 mm corresponds to a bandwidth of 4 nm. The excitation and emission slits were adjusted in all experiments to 0.375 mm, which is equivalent to a bandwidth of 1.5 nm. The use of the same bandwidth in the absorption and the emission experiments avoids distortions in the Lambert–Beer law.²³

The commercial spectrofluorometer was slightly modified in order to collect the emission at an angle of 180° with respect to the excitation beam (transmission configuration on *x*-axis). Figure 2 shows a photograph of the adapted setup. Despite

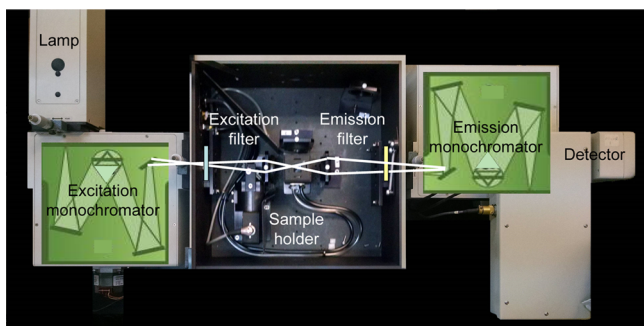


Figure 2. Commercial steady-state PTI QuantaMaster 4 CW fluorometer, adapted to collect the emission at 180° with respect to the excitation beam (transmission configuration).

having excitation and emission monochromators, some excitation light can pass through the sample and reach the detector, especially for low-absorbing samples. For this reason, it was necessary to interpose cutoff filters between both monochromators and the sample-holder. A Schott UG11 filter (2 mm thickness) was placed between the excitation source and the sample, in order to avoid that some spurious excitation light of long wavelengths reaches the sample. On the other hand, a Schott WG360 filter (2 mm thickness) was intercalated between the sample and the detector to prevent the excitation light from reaching the detector.

The use of convergent lenses and vertical slits in the experimental setup avoids: (a) the complete overlap between excitation and collection volumes and (b) the spatial coincidence between excitation and detection efficiencies. However, both conditions are reasonably met for small optical path lengths. In these cases, the small excitation and collection volumes properly overlap, and the differences between the spatial excitation and detection efficiencies become not significant, even independently of the absorption coefficient of the sample. For this reason, a 2 mm path quartz cell was used for both absorption and emission measurements. This length represents the longer path for which satisfactory results were obtained, in coincidence with an excitation beam practically homogeneous inside the cell, as can be seen with a naked eye in Figure 3a. On the other hand, unsatisfactory results were obtained for higher optical path-lengths, i.e. 10 mm, for which, coincidentally, an inhomogeneous excitation beam is observed (Figure 3b).

For a given molar dye concentration *C*, the experimentally observed fluorescence quantum yield in the *x* direction, $\Phi_{F,x}^{\text{obs}}(C)$, was obtained relative to the quantum yield of a diluted selected sample of concentration C_0 of the same compound in the same geometric configuration, $\Phi_{F,x}^{\text{obs}}(C_0)$. The calculation was performed in two different ways: (a) by considering the observed spectral photon irradiance in the *x*

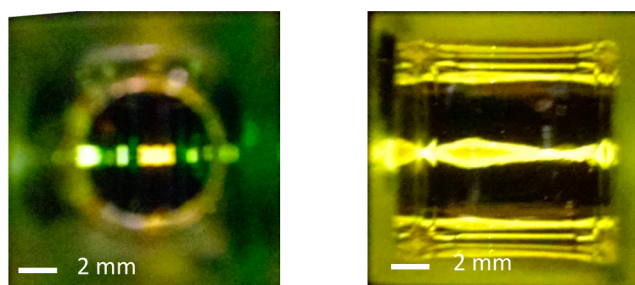


Figure 3. (a) Homogeneous excitation beam in a quartz cell of 2 mm optical path-length. (b) Inhomogeneous excitation beam in a quartz cell of 10 mm optical path-length.

direction $L_{p,x}^{\text{obs}}$ at a fixed emission wavelength, λ_F , in the red edge of the emission spectra:

$$\Phi_{F,x,\lambda_F}^{\text{obs}}(C) = \Phi_{F,x,\lambda_F}^{\text{obs}}(C_0) \frac{f_x(\lambda_0, C_0)}{f_x(\lambda_0, C)} \frac{L_{p,x}^{\text{obs}}(\lambda_0, \lambda_F, C)}{L_{p,x}^{\text{obs}}(\lambda_0, \lambda_F, C_0)} \quad (1)$$

and (b) by integrating $L_{p,x}^{\text{obs}}$ over the entire range of emission wavelengths λ :

$$\Phi_{F,x}^{\text{obs}}(C) = \Phi_{F,x}^{\text{obs}}(C_0) \frac{f_x(\lambda_0, C_0)}{f_x(\lambda_0, C)} \frac{\int_{\lambda} L_{p,x}^{\text{obs}}(\lambda_0, \lambda, C) d\lambda}{\int_{\lambda} L_{p,x}^{\text{obs}}(\lambda_0, \lambda, C_0) d\lambda} \quad (2)$$

In eqs 1 and 2, $f_x(\lambda_0, C)$ and $f_x(\lambda_0, C_0)$ represent the sample and the reference absorption factors respectively, expressed as

$$f_x(\lambda_0, C) = (1 - e^{-\varepsilon'(\lambda_0)C \cdot D})$$

$$f_x(\lambda_0, C_0) = (1 - e^{-\varepsilon'(\lambda_0)C_0 \cdot D}) \quad (3)$$

where $\varepsilon'(\lambda_0)$ is the napierian absorption coefficient at the excitation wavelength λ_0 (since $\varepsilon'(\lambda_0) = 2.303 \cdot \varepsilon(\lambda_0)$, with $\varepsilon(\lambda_0)$ the most commonly used decadic molar absorption coefficient) and *D* is the optical path-length.

Different blank spectra were subtracted to each dye fluorescence spectrum. The blank spectrum for each sample was obtained by multiplying the solvent spectrum by the corresponding $e^{-\varepsilon'(\lambda)C \cdot D}$ factor of the sample, in order to take into account the decreasing spurious light detected as the dye concentration increases.

The fluorescence quantum yield of DPA at diluted concentration in degassed toluene (refraction index $n = 1.497$) was determined as 1.00 ± 0.02 . In this case, the measurements were performed using a 90° configuration by choosing a 7.6×10^{-5} M acidic aqueous solution of QBS as reference ($n = 1.3391$, $\Phi_F(\text{QBS}) = 0.546$).³⁶

THEORETICAL APPROACH

A mathematical description of light emission is shown in this section. Two different phenomenological models are developed in order to reproduce both $L_{p,x}^{\text{obs}}$ and $\Phi_{F,x}^{\text{obs}}$ when they are affected by reabsorption. The models are based on the hypothesis that the emission of the dye—excluding events that can cause loss of excitation energy, such as quenching, molecular aggregation, and nonradiative energy transfer, among others—follows a linear dependence with the absorption factor along the entire concentration range. The symbols were chosen according to IUPAC recommendations for photochemistry terms.³⁷

Emission in the absence of reabsorption. Consider a monochromatic excitation beam impinging on an optical cell with parallel faces containing a homogeneous sample (e.g. dye solution). The polychromatic emitted light is detected in transmission geometry, i.e. at 180° with respect to the incident beam, as is shown in Figure 4.

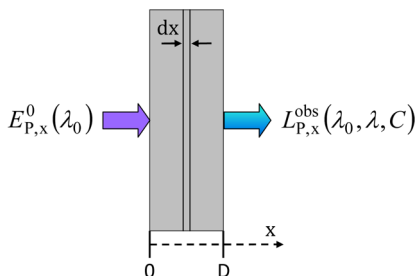


Figure 4. Geometry of the irradiation cell.

The excitation beam attenuates as it passes through the cell. The differential change in photon irradiance in the x direction, $dE_{p,x}$ is a measure of the corresponding differential population of excited molecules and can be expressed, according to the Lambert–Beer law, as

$$dE_{p,x}(\lambda_0, C, x) = -E_{p,x}^0(\lambda_0) \cdot \varepsilon'(\lambda_0) \cdot C \cdot e^{-\varepsilon'(\lambda_0)C \cdot x} dx \quad (4)$$

where $E_{p,x}^0$ and $E_{p,x}$ represent the excitation spectral photon irradiance, amount basis, at the surface of the cell and at a distance x from the surface, respectively.

Each differential of the excited population is able to generate a differential of light emission in all directions (isotropic). In the absence of reabsorption events, and assuming valid the Kasha-Vavilov rule,³⁷ this magnitude can be expressed for the x direction according to the following equation:

$$dL_{p,\Omega_x}(\lambda_0, \lambda, C, x) = \frac{1}{4\pi} \cdot \Phi_F \cdot \bar{L}_p(\lambda) \cdot dE_{p,x}(\lambda_0, C, x) \quad (5)$$

where L_{p,Ω_x} is the emission spectral photon radiance, amount basis, per solid angle unit in the x direction; Φ_F is the molecular emission quantum yield, and \bar{L}_p is the normalized emission spectral photon radiance, amount basis, satisfying $\int_{\lambda} \bar{L}_p(\lambda) d\lambda = 1$.

Integration of eq 5 between $x = 0$ and $x = D$ yields

$$L_{p,\Omega_x}(\lambda_0, \lambda, C) = \frac{1}{4\pi} \cdot E_{p,x}^0(\lambda_0) \cdot f_x(\lambda_0, C) \cdot \Phi_F \cdot \bar{L}_p(\lambda) \quad (6)$$

where a direct proportionality between the absorption factor and the intensity of the emission can be clearly perceived, in the absence of reabsorption.

The differential reabsorption model (DRM). Once the photons are generated by primary excitation, they are subjected to reabsorption as they travel through the sample. Equation 5 can be rewritten incorporating an exponential factor to account for the attenuation of the emission beam in the x direction, according to

$$dL_{p,\Omega_x}^{\text{DRM}}(\lambda_0, \lambda, C, x) = \frac{1}{4\pi} \cdot \Phi_F \cdot \bar{L}_p(\lambda) \cdot e^{-\varepsilon'(\lambda)C(D-x)} dE_{p,x}(\lambda_0, C, x) \quad (7)$$

Integration of eq 7 between $x = 0$ and $x = D$ leads to the following expression:

$$L_{p,\Omega_x}^{\text{DRM}}(\lambda_0, \lambda, C) = \frac{1}{4\pi} \cdot E_{p,x}^0(\lambda_0) \cdot \Phi_F \cdot \bar{L}_p(\lambda) \cdot \frac{\varepsilon'(\lambda_0) \cdot (e^{-\varepsilon'(\lambda)C \cdot D} - e^{-\varepsilon'(\lambda_0)C \cdot D})}{\varepsilon'(\lambda_0) - \varepsilon'(\lambda)} \quad (8)$$

which explicitly describes the effect of reabsorption in the x direction on the primary emission. Equations 6 and 8 can be combined, leading to

$$L_{p,\Omega_x}^{\text{DRM}}(\lambda_0, \lambda, C) = L_{p,\Omega_x}(\lambda_0, \lambda, C) \cdot \gamma_x^{\text{DRM}}(\lambda_0, \lambda, C) \quad (9)$$

with

$$\gamma_x^{\text{DRM}}(\lambda_0, \lambda, C) = \frac{\varepsilon'(\lambda_0)}{\varepsilon'(\lambda_0) - \varepsilon'(\lambda)} \cdot \frac{(e^{-\varepsilon'(\lambda)C \cdot D} - e^{-\varepsilon'(\lambda_0)C \cdot D})}{(1 - e^{-\varepsilon'(\lambda_0)C \cdot D})} \quad (10)$$

The factor $\gamma_x^{\text{DRM}}(\lambda_0, \lambda, C)$ relates the emission spectrum affected by reabsorption with the unaffected one, and can be interpreted as the mean probability that a primary photon emitted with a wavelength λ , after excitation at λ_0 , escapes out of the sample in the x direction. For practical purposes, it can be conveniently expressed in terms of absorbance as

$$\gamma_x^{\text{DRM}}(\lambda_0, \lambda, C) = \frac{A(\lambda_0, C)}{A(\lambda_0, C) - A(\lambda, C)} \cdot \frac{(10^{-A(\lambda, C)} - 10^{-A(\lambda_0, C)})}{(1 - 10^{-A(\lambda_0, C)})} \quad (11)$$

since $A(\lambda, C) = \varepsilon(\lambda)C \cdot D$ and $A(\lambda_0, C) = \varepsilon(\lambda_0)C \cdot D$.

The factor $\gamma_x^{\text{DRM}}(\lambda_0, \lambda, C)$ is identical to that reported by Budó and Ketskeméty⁸ for the same geometry of detection, and similar to those obtained by Budó and Ketskeméty,⁸ Rohatgi and Singhal,¹¹ and Lopez Arbeloa¹³ for other geometries.

The median reabsorption model (MRM). A different strategy to simplify the mathematical approach considers that all the excited molecules are located in a representative surface, \bar{S} , perpendicular to the excitation beam inside the cell. The distance from the front edge of the cell to this surface, x_M , is proposed such that it splits the excited states population into two equal parts, by satisfying:

$$\int_0^{x_M} dE_{p,x}(\lambda_0, \lambda, C) = \int_{x_M}^D dE_{p,x}(\lambda_0, \lambda, C) \quad (12)$$

and can be determined as

$$x_M(\lambda_0, C) = -\frac{1}{\varepsilon'(\lambda_0)C} \ln\left(\frac{1 + e^{-\varepsilon'(\lambda_0)C \cdot D}}{2}\right) \quad (13)$$

or, expressed in terms of absorbance:

$$x_M(\lambda_0, C) = -\frac{D}{2.303A(\lambda_0, C)} \ln\left(\frac{1 + 10^{-A(\lambda_0, C)}}{2}\right) \quad (14)$$

Under this assumption, it is considered that all the emitted light is generated from \bar{S} . An expression for the emission affected by reabsorption in the x direction can be achieved by modifying eq 6 as follows:

$$L_{p,\Omega_x}^{\text{MRM}}(\lambda_0, \lambda, C) = \frac{1}{4\pi} \cdot E_{p,x}^0(\lambda_0) \cdot f_x(\lambda_0, C) \cdot \Phi_F \cdot \bar{L}_p(\lambda) \cdot e^{-\varepsilon'(\lambda)C(D-x_M)} \quad (15)$$

yielding

$$L_{p,\Omega_x}^{\text{MRM}}(\lambda_0, \lambda, C) = L_{p,\Omega_x}(\lambda_0, \lambda, C) \cdot \gamma_x^{\text{MRM}}(\lambda_0, \lambda, C) \quad (16)$$

with:

$$\gamma_x^{\text{MRM}}(\lambda_0, \lambda, C) = e^{-\varepsilon'(\lambda)C \cdot D} \left(\frac{2}{1 + e^{\varepsilon'(\lambda_0)C \cdot D}} \right)^{\varepsilon'(\lambda)/\varepsilon'(\lambda_0)} \quad (17)$$

or, expressed in terms of absorbance:

$$\gamma_x^{\text{MRM}}(\lambda_0, \lambda, C) = 10^{-A(\lambda,C)} \left(\frac{2}{1 + 10^{A(\lambda_0,C)}} \right)^{A(\lambda,C)/A(\lambda_0,C)} \quad (18)$$

It is interesting to note that both eqs 11 and 18 tend to $10^{-A(\lambda,C)}$ when $A(\lambda_0,C) \rightarrow \infty$, indicating that $\gamma_x^{\text{DRM}}(\lambda_0, \lambda, C)$ and $\gamma_x^{\text{MRM}}(\lambda_0, \lambda, C)$ become independent of the absorption at the excitation wavelength for high absorbances.

The assumption that all the emitted light comes from a surface located at x_M provides a simplified point of view for the reabsorption events in the x direction. As such, this approach will be useful in the next section to explain why re-emission is not detected in this geometric configuration.

Calculation of emission spectra and quantum yields using the reabsorption models. The values obtained from eqs 6, 9, and 16 must be weighted by the solid angle of detection, $\Omega_{\text{det}}(x)$, in order to establish a proper comparison between experimental $L_{p,x}^{\text{obs}}(\lambda_0, \lambda, C)$ and calculated spectra $L_{p,x}(\lambda_0, \lambda, C)$, $L_{p,x}^{\text{DRM}}(\lambda_0, \lambda, C)$, and $L_{p,x}^{\text{MRM}}(\lambda_0, \lambda, C)$. In principle, $\Omega_{\text{det}}(x)$ depends on the position at which the emission is generated inside the cell. However, the geometry of the experimental setup, in which $D = 0.2 \text{ cm} \ll 5 \text{ cm} = L$, the distance to the optical detection lens, makes $\Omega_{\text{det}}(x) \approx \Omega_{\text{det}}$ a very good approximation. This feature allows the replacement of $L_{p,x}$ instead of L_{p,Ω_x} in eqs 9 and 16.

The calculation of the emission spectra affected by reabsorption was performed as follows: (a) an experimental emission spectrum from a dilute sample, $L_{p,x}^{\text{obs}}(\lambda_0, \lambda, C_0)$ was selected; (b) this spectrum was divided by $f_x(\lambda_0, C_0)$ and multiplied by $f_x(\lambda_0, C)$ in order to obtain $L_{p,x}(\lambda_0, \lambda, C)$ for the entire concentration range; (c) each $L_{p,x}(\lambda_0, \lambda, C)$ was then multiplied by $\gamma_x^{\text{DRM}}(\lambda_0, \lambda, C)$ or $\gamma_x^{\text{MRM}}(\lambda_0, \lambda, C)$ to obtain $L_{p,x}^{\text{DRM}}(\lambda_0, \lambda, C)$ and $L_{p,x}^{\text{MRM}}(\lambda_0, \lambda, C)$, respectively.

The calculation of the emission quantum yields in the x direction affected by reabsorption, $\Phi_{F,x}^{\text{DRM}}$ and $\Phi_{F,x}^{\text{MRM}}$, was achieved by dividing eqs 9 and 16 by $\int_{\lambda} L_{p,x}(\lambda_0, \lambda, C) d\lambda$, and subsequent integration over the entire range of emission wavelengths. This leads to the following expressions:

$$\Phi_{F,x}^{\text{DRM}}(C) = \Phi_F \cdot [1 - P_{0,x}^{\text{DRM}}(\lambda_0, C)] \quad (19)$$

$$\Phi_{F,x}^{\text{MRM}}(C) = \Phi_F \cdot [1 - P_{0,x}^{\text{MRM}}(\lambda_0, C)] \quad (20)$$

where $P_{0,x}^{\text{DRM}}$ and $P_{0,x}^{\text{MRM}}$ represent the mean probabilities of reabsorption in the x direction integrated over the emission spectrum, defined as

$$P_{0,x}^{\text{DRM}}(\lambda_0, C) = \int \bar{L}_p(\lambda) \cdot [1 - \gamma_x^{\text{DRM}}(\lambda_0, \lambda, C)] \cdot d\lambda \quad (21)$$

$$P_{0,x}^{\text{MRM}}(\lambda_0, C) = \int \bar{L}_p(\lambda) \cdot [1 - \gamma_x^{\text{MRM}}(\lambda_0, \lambda, C)] \cdot d\lambda \quad (22)$$

Equations 19 and 20 are similar to that reported by Birks,²⁶ except for the procedure through which $P_{0,x}^{\text{DRM}}$ and $P_{0,x}^{\text{MRM}}$ are calculated. It is important to note that these equations do not include a positive re-emission term $P_0 \cdot \Phi_F$, appearing in the expressions used for the measurements with integrating spheres.^{38–40} Once calculated, $\Phi_{F,x}^{\text{DRM}}$ and $\Phi_{F,x}^{\text{MRM}}$ values should be compared with $\Phi_{F,x}^{\text{obs}}$ to verify that the models accurately reproduce the experimental results.

RESULTS AND DISCUSSION

Figure 5 shows $f_x(\lambda_0, C)$ of DPA in toluene as a function of λ_0 , for samples ranging between 1.12×10^{-5} and 1.30×10^{-2} M.

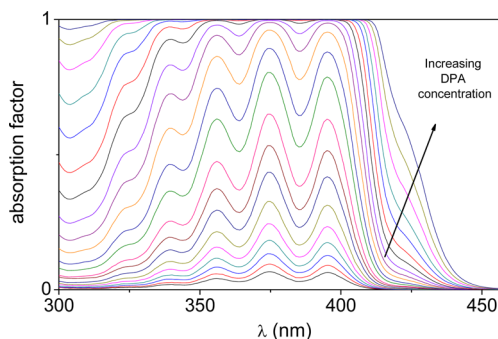


Figure 5. Absorption factor, $f_x(\lambda_0, C)$, of DPA in toluene, from 1.12×10^{-5} M to 1.30×10^{-2} M and an optical path-length of 0.2 cm.

For concentration values higher than 2.22×10^{-3} M, the amount of absorbed light at $\lambda_0 = 350$ nm reaches unity, indicating the total absorption of the excitation beam for an optical path-length of 0.2 cm.

The steady-state fluorescence spectra of the same set of DPA solutions, obtained by exciting at 350 nm, are shown in Figure 6. The emission intensity at the red shoulder increases as the

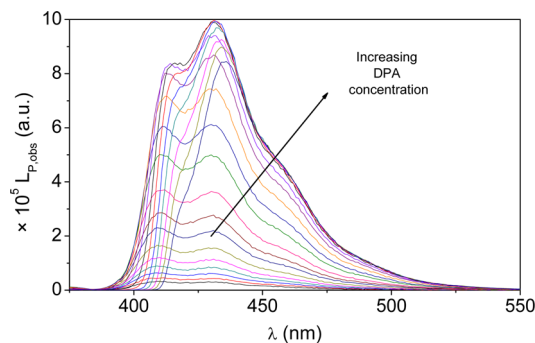


Figure 6. Steady-state fluorescence spectra of DPA in toluene, from 1.12×10^{-5} to 1.30×10^{-2} M and an optical path-length of 0.2 cm.

concentration increases, reaching a maximum value for concentrations above 2.22×10^{-3} M. On the other hand, the spectral shape changes at the blue edge as the concentration increases. These changes are located in the overlap region between the absorption and the emission spectra, and can be attributed to reabsorption. It is interesting to note that, if the reabsorbed radiation is re-emitted and further collected, the changes at the blue edge of the spectra should be accompanied by proportional changes at the red edge, since $\Phi_F(\text{DPA}) = 1$.

This is not observed in the experiments, indicating that the re-emitted light is actually not detected.

Results for $\Phi_{F,x,\lambda_F}^{\text{obs}}$ obtained from eq 1 at $\lambda_F = 460$ nm, are plotted in Figure 7 as a function of DPA concentration. It is

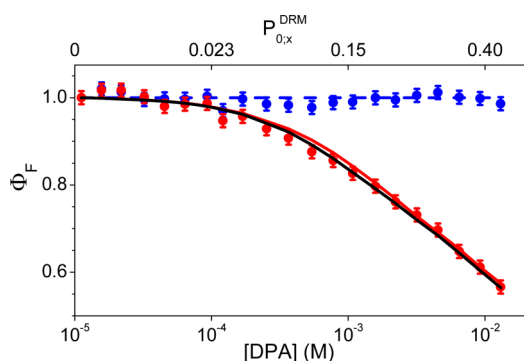


Figure 7. $\Phi_{F,x,\lambda_F}^{\text{obs}}$ (blue dots), $\Phi_{F,x}^{\text{obs}}$ (red dots), Φ_F (blue line), $\Phi_{F,x}^{\text{DRM}}$ (red line), and $\Phi_{F,x}^{\text{MRM}}$ (black line), as a function of DPA concentration and $P_{0,x}^{\text{DRM}}$.

observed that $\Phi_{F,x,\lambda_F}^{\text{obs}}$ remains constant for the entire concentration range. Clearly, the emission at 460 nm is not affected by reabsorption, because the DPA absorbance is negligible at this wavelength, even for the highest concentrations. In the same figure, results for $\Phi_{F,x}^{\text{obs}}$ calculated from eq 2 by integration over the entire emission spectra, are also plotted. It is observed that $\Phi_{F,x}^{\text{obs}}$ decreases as the concentration increases. The lowering of the total emission caused by reabsorption, and the fact that the re-emitted light is not detected, are consistent with the observed trends.

In order to quantitatively describe the effects caused by reabsorption in the x direction on the fluorescence spectra and quantum yields, $\gamma_x^{\text{DRM}}(\lambda_0, \lambda, C)$ and $\gamma_x^{\text{MRM}}(\lambda_0, \lambda, C)$ were calculated for the entire concentration range. Figure 8 shows the results as

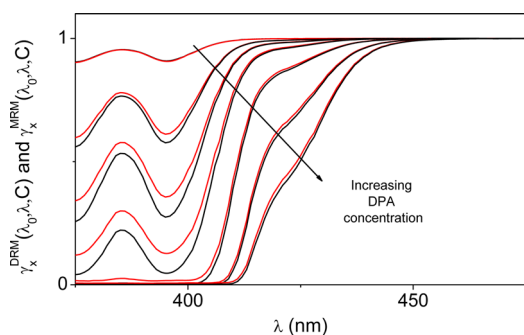


Figure 8. $\gamma_x^{\text{DRM}}(\lambda_0, \lambda, C)$ (red lines) and $\gamma_x^{\text{MRM}}(\lambda_0, \lambda, C)$ (black lines) for toluene DPA solutions of 3.23×10^{-5} M; 1.69×10^{-4} M; 3.66×10^{-4} M; 7.77×10^{-4} M; 2.22×10^{-3} M; 6.49×10^{-3} M; and 1.30×10^{-2} M.

a function of λ for some selected concentrations. It is observed that the shape and intensity of the functions, calculated using the DRM and the MRM, agree very well for low and high concentrations, but differ slightly at intermediate concentrations, particularly for wavelengths between 380 and 400 nm. As will be shown below, the differences observed at these wavelengths do not produce significant effects on the subsequent calculations, since they are located in a spectral region where the fluorescence intensity of the dye is rather low.

The agreement between reabsorption calculations and experimental data can be tested by reproducing $L_{p,x}^{\text{obs}}$ for the entire concentration range. For this purpose, the emission spectrum of the DPA solution of 6.40×10^{-5} M was selected as $L_{p,x}^{\text{obs}}(\lambda_0, \lambda, C_0)$. This sample constitutes the highest concentration for which reabsorption is negligible, taking $P_{0,x}^{\text{DRM}} < 0.02$ as an upper limit. Figure 9 shows that both calculated spectra,

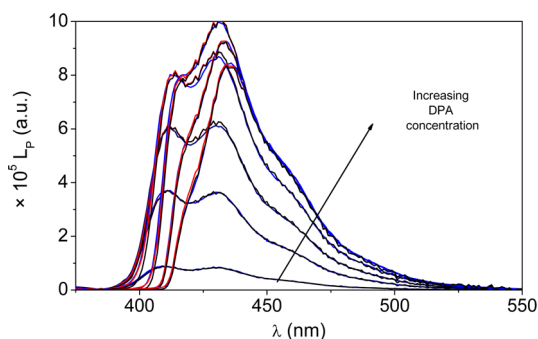


Figure 9. Experimental $L_{p,x}^{\text{obs}}(\lambda_0, \lambda, C)$ (blue lines) and calculated $L_{p,x}^{\text{DRM}}(\lambda_0, \lambda, C)$ (red lines) and $L_{p,x}^{\text{MRM}}(\lambda_0, \lambda, C)$ (black lines) fluorescence spectra of DPA in toluene, for an optical-path length of 0.2 cm and concentration values of 3.23×10^{-5} M; 1.69×10^{-4} M; 3.66×10^{-4} M; 7.77×10^{-4} M; 2.22×10^{-3} M; 6.49×10^{-3} M; and 1.30×10^{-2} M.

$L_{p,x}^{\text{DRM}}(\lambda_0, \lambda, C)$ and $L_{p,x}^{\text{MRM}}(\lambda_0, \lambda, C)$, agree very well with the experimental data. Results for $\Phi_{F,x}^{\text{DRM}}$ and $\Phi_{F,x}^{\text{MRM}}$, shown in Figure 7, also reproduce quite well the experimental trend of $\Phi_{F,x}^{\text{obs}}$. The discrepancy between $\gamma_x^{\text{DRM}}(\lambda_0, \lambda, C)$ and $\gamma_x^{\text{MRM}}(\lambda_0, \lambda, C)$ at intermediate concentrations (see Figure 8) represents a difference of less than 1% between $P_{0,x}^{\text{DRM}}$ and $P_{0,x}^{\text{MRM}}$. These results confirm that both models show no significant differences with the experimental uncertainty. Table 1 summarizes some experimental and calculated magnitudes.

Considering that only reabsorption corrections are necessary to reproduce experimental results, one can wonder why re-emission is not observed in the experiments. The answer to this question lies in the fact that the fraction of the primary emitted light that is capable to be reabsorbed within the detection volume and, therefore, re-emitted and detectable, P_{eff} should be not significant. The unidirectional approach used so far does not seem suitable to calculate P_{eff} because the almost cylindrical detection volume has an estimated radius, $r \sim 0.04$ cm, which is not negligible compared to D . As such, a different strategy, based on the MRM, will be developed below to estimate this parameter.

It is important to first note that primary emission occurs after a monochromatic excitation at λ_0 , whereas re-emission occurs upon a polychromatic excitation (reabsorption). As such, a mean napierian absorption coefficient in the x direction, $\bar{\epsilon}'$, can be obtained for the reabsorption process, as

$$\bar{\epsilon}' = -\frac{1}{C \cdot D} \ln(1 - P_{0,x}^{\text{MRM}}) \quad (23)$$

The replacement of $\epsilon'(\lambda_0)$ and D by $\bar{\epsilon}'$ and $(D - x_M)$ in eq 13 allows the calculation of x_M^R , the mean distance at which the primary emission, originated from \bar{S} , is reabsorbed in the x direction. This distance and the radius of the cylindrical detection volume r allow the calculation of a solid angle Ω_R for which the emission of the re-excited molecules is likely to be detected, according to

Table 1. Experimental and Calculated Photophysical Parameters of DPA in Toluene^a

[DPA]/M	$\Phi_{F,x,\lambda_F}^{\text{obs}}$	$\Phi_{F,x}^{\text{obs}}$	$P_{0,x}^{\text{DRM}}$	$P_{0,x}^{\text{MRM}}$	$\Phi_{F,x}^{\text{DRM}}$	$\Phi_{F,x}^{\text{MRM}}$
1.12×10^{-5}	1.00	1.00	0.003	0.005	1.00	1.00
1.57×10^{-5}	1.02	1.02	0.004	0.007	1.00	1.00
2.19×10^{-5}	1.01	1.02	0.006	0.008	1.00	1.00
3.23×10^{-5}	1.00	1.00	0.008	0.011	0.99	0.99
4.54×10^{-5}	1.00	0.98	0.011	0.014	0.99	0.99
6.40×10^{-5}	1.00	0.99	0.015	0.018	0.99	0.99
9.30×10^{-5}	1.00	0.99	0.022	0.025	0.98	0.98
1.21×10^{-4}	0.97	0.95	0.029	0.033	0.97	0.97
1.69×10^{-4}	1.00	0.96	0.038	0.043	0.96	0.96
2.53×10^{-4}	0.99	0.93	0.057	0.064	0.95	0.94
3.66×10^{-4}	0.98	0.91	0.074	0.084	0.93	0.92
5.41×10^{-4}	0.98	0.88	0.100	0.113	0.90	0.89
7.77×10^{-4}	0.99	0.86	0.128	0.144	0.87	0.86
1.08×10^{-3}	0.99	0.83	0.160	0.176	0.84	0.83
1.58×10^{-3}	1.00	0.80	0.198	0.213	0.80	0.79
2.22×10^{-3}	0.99	0.76	0.234	0.246	0.77	0.76
3.17×10^{-3}	1.01	0.73	0.274	0.284	0.73	0.72
4.52×10^{-3}	1.01	0.70	0.311	0.320	0.69	0.68
6.49×10^{-3}	1.00	0.65	0.349	0.359	0.65	0.64
9.21×10^{-3}	1.00	0.61	0.390	0.400	0.61	0.60
1.30×10^{-2}	0.99	0.57	0.427	0.439	0.57	0.56

^aMolar dye concentration, [DPA]; experimental fluorescence quantum yield in the x direction at $\lambda_F = 460$ nm, $\Phi_{F,x,\lambda_F}^{\text{obs}}$; integrated experimental fluorescence quantum yield in the x direction, $\Phi_{F,x}^{\text{obs}}$; mean reabsorption probability in the x direction from the differential reabsorption model, $P_{0,x}^{\text{DRM}}$; mean reabsorption probability in the x direction from the median reabsorption model, $P_{0,x}^{\text{MRM}}$; calculated fluorescence quantum yield in the x direction from the differential reabsorption model, $\Phi_{F,x}^{\text{DRM}}$; calculated fluorescence quantum yield in the x direction from the median reabsorption model, $\Phi_{F,x}^{\text{MRM}}$.

$$\frac{\Omega_R}{4\pi} = \frac{1}{2} \left(1 - \frac{x_M^R}{\sqrt{(x_M^R)^2 + r^2}} \right) \quad (24)$$

As a rough estimate, it can be assumed the same Ω_R value for the emissions originated at any point of \vec{s} . Under these circumstances, the re-emission of first generation of a highly absorbing sample can be approximated by

$$L_{p,\Omega,1}(\lambda_0, \lambda, C) \approx L_{p,\Omega}(\lambda_0, \lambda, C) \cdot \left[\frac{\Omega_R}{4\pi} \cdot P_0(\lambda_0, C) \cdot \Phi_F \cdot 10^{-A(\lambda,C)} \right] \quad (25)$$

where the factor between brackets relates the amount of re-emitted radiation of first generation with the one emitted from the direct excitation at λ_0 . The expression for P_{eff} now becomes

$$P_{\text{eff}}(\lambda_0, C) = \frac{\Omega_R}{4\pi} \cdot P_0(\lambda_0, C) \quad (26)$$

For the most concentrated DPA solution, $\bar{e} \approx 222 \text{ M}^{-1} \text{ cm}^{-1}$, yielding $x_M^R = 0.084 \text{ cm}$, $\Omega_R/4\pi \approx 0.049$, and $P_{\text{eff}} \sim 0.02$. As expected, lower values for this parameter are obtained for lower DPA concentrations.

The latter calculation indicates that re-emission is hardly detected in this geometric configuration because it represents $\sim 2\%$ of the total emission detected. However, this fact does not rule out other possibilities of quantitative detection of re-emitted light by using another geometric configuration, as was

previously reported some time ago by Budó et al.⁶ and recently confirmed by Kušba and co-workers.⁴¹

CONCLUSIONS

A new methodology to acquire emission spectra and quantum yields of highly absorbing solutions is presented. The experimental measurements were performed in a commercial spectrofluorometer adapted to transmission geometry, in which the detection is located at 180° with respect to the excitation beam. This feature, along with the use of a short path-length, avoids problems caused by excitation or primary inner-filter effects, since it ensures the complete overlap between excitation and detection volumes. The methodology is complemented with two mathematical models that rationalize distortions in experimental spectra. Although the technique was used for liquid faces, it can also be applied on films and solid samples provided they are not optically dense.

The results indicate that reabsorption corrections accurately reproduce the experimental data and that the molecular emission spectra and quantum yields of the samples can be recovered. Moreover, it was verified that re-emission effects are not detected using the present experimental geometry, allowing the direct calculation of the emission quantum yields from intensity data at the red side of the emission spectra. The latter finding is particularly relevant because quantum yields of highly concentrated solutions can be obtained without the need of any mathematical correction. As such, its concentration dependence, if any, could be directly attributed to other quenching mechanisms, such as molecular aggregation and nonradiative energy transfer.

The technique was developed, in principle, for samples having a single substance capable of absorbing and emitting radiation. Eventually, it can be simply reformulated for samples combining n absorbing (but nonemitting) entities. In such cases, the absorption factor of the corresponding emitting species must be expressed as $[A_1(\lambda_0, C)/A_T(\lambda_0, C_1, C_2, \dots, C_n)] [1 - 10^{-A_T(\lambda_0, C_1, C_2, \dots, C_n)}]$, where A_1 and A_T represent the emitting substance and total absorbances, respectively. For samples containing more than one emitting species, the method cannot be adapted in a simple fashion; such treatment clearly deserves a more detailed analysis, which is beyond the scope of the present paper.

The method presented here, simpler and more robust compared with other alternatives, can be applied in commercial spectrofluorometers after slightly geometrical modifications. The upper concentration limit to be used is determined, in principle, by the solubility of the dyes. However, in such cases, it must be ensured that the re-emission reaching the detector remains negligible. Compared with *front-face* and 90° conventional measurements, the technique offers the advantage that primary inner-filter effects are avoided.

AUTHOR INFORMATION

Corresponding Author

*Tel: +54 11 6772 7198. Fax: +54 11 6772 7886. E-mail: mirenda@cnea.gov.ar.

ORCID

Martín Mirenda: 0000-0003-0478-5178

Author Contributions

[†]H.B.R. and M.M. contributed equally.

Notes

The authors declare no competing financial interest.

ACKNOWLEDGMENTS

Funding was obtained from ANPCyT (PICT 2011-2348) and CONICET (PIP 11220130100795CO). D.R. has a postdoctoral fellowship from CONICET. H.B.R. and M.M. are staff members of CONICET. H.B.R. and M.M. would like to express special thanks to Prof. Enrique San Román for his kind support and guidance on photochemical research, and to whom this article is dedicated. Discussions with Maria Laura Japas and Daniel Laria are greatly acknowledged.

REFERENCES

- (1) Knut, R. *Fluorescence Quantum Yields: Methods of Determination and Standards*; Springer: Berlin, 2008; pp 101–145.
- (2) Würth, C.; Grabolle, M.; Pauli, J.; Spieles, M.; Resch-Genger, U. *Nat. Protoc.* **2013**, *8*, 1535–1550.
- (3) Miller, J. N. Chapter 5: Inner filter effects, sample cells and their geometry in fluorescence spectrometry. *Standards in Fluorescence Spectrometry*; Springer: Netherlands, 1981; pp 27–43.
- (4) Birks, J. B. *J. Res. Natl. Bur. Stand., Sect. A* **1976**, *80A*, 389–399.
- (5) Vavilov, S. I. *Z. Phys.* **1925**, *31*, 750–764.
- (6) Budó, A.; Dombi, J.; Szollosy, L. *Acta Phys. Chem.* **1956**, *2*, 18–27.
- (7) Budó, A.; Ketskeméty, I. *J. Chem. Phys.* **1956**, *25*, 595–596.
- (8) Budó, A.; Ketskeméty, I. *Acta Phys. Acad. Sci. Hung.* **1957**, *7*, 207–223.
- (9) Melhuish, W. H. *J. Phys. Chem.* **1961**, *65*, 229–235.
- (10) Rohatgi, K. K.; Singhal, G. S. *Anal. Chem.* **1962**, *34*, 1702–1706.
- (11) Rohatgi, K. K.; Singhal, G. S. *Photochem. Photobiol.* **1968**, *7*, 361–367.
- (12) Eisinger, J.; Flores, J. *Anal. Biochem.* **1979**, *94*, 15–21.
- (13) Lopez Arbeloa, I. *J. Photochem.* **1980**, *14*, 97–105.
- (14) Vieira Ferreira, L. F.; Costa, S. M. B.; Pereira, E. J. *J. Photochem. Photobiol., A* **1991**, *55*, 361–376.
- (15) Weber, G.; Teale, F. W. J. *Trans. Faraday Soc.* **1957**, *53*, 646–655.
- (16) Parker, C. A.; Rees, W. T. *Analyst* **1960**, *85*, 587–600.
- (17) Holland, J. F.; Teets, R. E.; Kelly, P. M.; Timnick, A. *Anal. Chem.* **1977**, *49*, 706–710.
- (18) Novák, A. *Collect. Czech. Chem. Commun.* **1978**, *43*, 2869–2877.
- (19) Lutz, H.-P.; Luisi, P. L. *Helv. Chim. Acta* **1983**, *66*, 1929–1935.
- (20) Kubista, M.; Sjöback, R.; Eriksson, S.; Albinsson, B. *Analyst* **1994**, *119*, 417–419.
- (21) MacDonald, B. C.; Lvin, S. J.; Patterson, H. *Anal. Chim. Acta* **1997**, *338*, 155–162.
- (22) Gu, Q.; Kenny, J. E. *Anal. Chem.* **2009**, *81*, 420–426.
- (23) Gu, Q. Improvement of corrections for fluorescence inner filter effects under non-ideal beam conditions based on effective geometric parameters. Ph.D. Thesis, Tufts University, Boston, 2007.
- (24) Fonin, A. V.; Sulatskaya, A. I.; Kutnetsova, I. M.; Turoverov, K. *PLoS One* **2014**, *9*, e103878.
- (25) Parker, C. A. *Photoluminescence of solutions*; Elsevier: London, 1968.
- (26) Birks, J. B. *Photophysics of aromatic molecules*, 1st ed.; John Wiley & Sons Ltd: London, 1970.
- (27) Fletcher, K. A.; Fakayode, S. O.; Lowry, M.; Tucker, S. A.; Neal, S. L.; Kimaru, I. W.; McCarroll, M. E.; Patonay, G.; Oldham, P. B.; Rusin, O.; Strongin, R. M.; Warner, I. M. *Anal. Chem.* **2006**, *78*, 4047–4068.
- (28) Chamberlain, J. *The Analysis of Drugs in Biological Fluids*, 2nd ed.; CRC Press: Boca Raton, FL, 1995.
- (29) Lanzani, G. *Photophysics of molecular materials: from single molecules to single crystals*; Wiley-VCH: Weinheim, 2005.
- (30) Izawa, H.; Wakizono, S.; Kadokawa, J.-i. *Chem. Commun.* **2010**, *46*, 6359–6361.
- (31) Chen, X.-W.; Liu, J.-W.; Wang, J.-H. *J. Phys. Chem. B* **2011**, *115*, 1524–1530.
- (32) Heinrich, G.; Schoof, S.; Gusten, H. *J. Photochem.* **1974**, *3*, 315–320.
- (33) Martinho, J. M. G.; Macanita, A. L.; Berberán-Santos, M. N. *J. Chem. Phys.* **1989**, *90*, 53–59.
- (34) Gray, V.; Dzebo, D.; Lundin, A.; Alborzpour, J.; Abrahamsson, M.; Albinsson, B.; Moth-Poulsen, K. *J. Mater. Chem. C* **2015**, *3*, 11111–11121.
- (35) DeVol, T. A.; Wehe, D. K.; Knoll, G. F. *Nucl. Instrum. Methods Phys. Res., Sect. A* **1994**, *348*, 156–162.
- (36) Dawson, W. R.; Windsor, M. W. *J. Phys. Chem.* **1968**, *72*, 3251–3260.
- (37) Braslavsky, S. E. *Pure Appl. Chem.* **2007**, *79*, 293–465.
- (38) Suzuki, K.; Kobayashi, A.; Kaneko, S.; Takehira, K.; Yoshihara, T.; Ishida, H.; Shiina, Y.; Oishi, S.; Tobita, S. *Phys. Chem. Chem. Phys.* **2009**, *11*, 9850–9860.
- (39) Lagorio, G.; Dicelio, L.; Litter, M.; San Roman, E. *J. Chem. Soc., Faraday Trans.* **1998**, *94*, 419–425.
- (40) Ahn, T. S.; Al-Kaysi, R. O.; Müller, A. M.; Wentz, K. M.; Bardeen, C. J. *Rev. Sci. Instrum.* **2007**, *78*, 086105.
- (41) Kušba, J.; Grajek, H.; Gryczynski, I. *Methods Appl. Fluoresc.* **2014**, *2*, 015001.